Hindawi Publishing Corporation
Journal of Nanomaterials
Volume 2016, Article ID 4292316, 10 pages
http://dx.doi.org/10.1155/2016/4292316

Research Article

Carbon Dioxide Adsorption in Nanopores of Coconut Shell Chars for Pore Characterization and the Analysis of Adsorption Kinetics

Chaiyot Tangsathitkulchai, Supunnee Junpirom, and Juejun Katesa

School of Chemical Engineering, Institute of Engineering, Suranaree University of Technology, Muang District, Nakhon Ratchasima 30000, Thailand

Correspondence should be addressed to Chaiyot Tangsathitkulchai; chaiyot@sut.ac.th

Received 20 August 2016; Accepted 27 November 2016

Academic Editor: Ajayan Vinu

The uptake data of CO_2 adsorption at 273 K by coconut shell chars prepared at various carbonization temperatures from 250 to 550°C were used for characterizing pore texture of chars as well as the analysis of CO_2 adsorption kinetics. The equilibrium isotherms were used to determine the porous texture of chars, employing the DR equation and GCMC simulation. It was found that all the test chars contain micropores of a size range from 0.8 to 2.2 nm with the pore size distribution becoming wider for char prepared at a higher carbonization temperature. Porous properties of chars, including surface area, total pore volume, and the average pore size, appear to increase with an increasing carbonization temperature. The analysis of CO_2 uptake during the transient measurement of isotherms revealed that the kinetics of CO_2 adsorption is governed by the internal diffusional transport of the adsorptive molecules. The effective pore diffusivity characterizing this transport process increases with increasing CO_2 loading and passes through a maximum at a certain loading. This maximum pore diffusivity shifts to a higher value as the carbonization temperature is increased. A semiempirical equation was developed to correlate the effective pore diffusivity of CO_2 with the equilibrium adsorption loading and its predictive capability is satisfactory.

1. Introduction

Pyrolysis is a simple and attractive thermal process for converting biomass into various fuel sources, including low calorific-value gases, liquid biooil, and solid carbon char, as well as a variety of useful chemical species [1–4]. The solid char in particular can be alternatively used as a primary low-cost adsorbent [5, 6] or further activated to produce a highly porous activated carbon which finds many applications in the separation and purification processes [7, 8]. The yield, physicochemical properties, and pore characteristics of the char product are normally determined as part of the evaluation of the pyrolysis process. In general, the nitrogen gas adsorption is the most widely used method for the characterization of porous adsorbents [9, 10]. However, this technique is not so practical and may lead to erroneous results when it is applied for biomass chars; for example, the decrease of the adsorbed amount with increasing pressure could be observed or the time to reach adsorption equilibrium is extremely long (the so-called activated diffusion effect) [11]. This is partly explained by the low diffusion rate of the N_2 probe molecule at 77 K inside the narrow pores of the poorly connected pore structure of char. To solve this problem, carbon dioxide adsorption at 273 K is a preferred choice [12] because the higher adsorption temperature of CO_2 enables the adsorptive molecules to enter more quickly into the narrow micropores of the char. Apart from the required data on equilibrium isotherms for characterizing porous properties of chars, information on the transport of carbon dioxide inside the internal pores is also important for the design of a thermal conversion system [13]. In addition, the diffusion of carbon dioxide in chars with different pore structures can have a significant influence on the reactivity of char gasification in the production of syngas and activated carbon [14, 15].

This work presents a standard analysis of CO_2 uptake data derived from gravimetric adsorption equipment for the simultaneous determination of both pore texture of coconut shell chars and the kinetics of CO_2 adsorption. Chars prepared from the carbonization of coconut shell in an inert atmosphere of nitrogen at temperatures over the range from 250 to 550°C were investigated.

2. Materials and Methods

2.1. Raw Materials. Coconut shell was used as a raw material in this work. The as-received coconut shell was first dried in an electric oven at 110°C overnight and the dry sample was crushed and sieved to obtain a screen size fraction of 12 × 16 mesh, with the average particle size of 1.44 mm. The prepared sample was kept for proximate, ultimate, and thermal analyses, as well as for char preparation.

2.2. Coconut Shell Characterization. The coconut shell sample was analyzed for the proximate analysis on a dry basis, namely, the volatile matter, the fixed carbon content, and the ash content, by employing a thermogravimetric analyzer (TGA) (model SDT 2960, TA Instruments, USA) with the analysis procedure being reported elsewhere [14]. The elemental or ultimate analysis of the coconut shell was analyzed by a CHNS analyzer (model PE 2400 Series II, Perkin Elmer, USA).

Thermal decomposition behavior of the coconut shell was determined using the same thermogravimetric analyzer by heating the sample under a constant flow of nitrogen gas from room temperature to the final temperature of 750°C and the sample weight loss was monitored.

2.3. Char Preparation. About 30 g of coconut shell sample was heated in a horizontal tube furnace (model CTF 12/75/700, Carbolite, UK) under a constant flow of N_2 at the rate of 100 cm^3/min. In all runs, the heating temperature was programmed to increase from room temperature to the desired carbonization temperature at the heating rate of 5°C/min and held at this temperature for 2 h. After that, the furnace was turned off and the char was cooled inside the furnace to room temperature under the flow of N_2. The carbonization temperature studied was varied in the range from 250 to 550°C.

2.4. Char Characterization. The derived char products were characterized for the proximate analysis and their images of surface morphology were ascertained with a scanning electron microscopy instrument (model JEOL JSM-6400, JEOL Ltd., Japan). The true densities of the prepared chars were measured with a helium pycnometer (model AccuPyc 1330, Micromeritics, USA).

2.5. Carbon Dioxide Adsorption. Investigation of CO_2 adsorption by solid chars from coconut shell was performed in an Intelligent Gravimetric Analyzer (IGA) (Hiden Analytical, UK). Initially, the char sample weighing about 0.2 g was outgassed at 300°C for 10 h at a vacuum pressure of 75 mmHg. Next, the adsorption of CO_2 was carried out at 273 K by dosing CO_2 at a specified pressure and the increasing amount of CO_2 adsorbed was recorded as a function of time until the equilibrium was established. The measurement was then repeated for a number of increasing pressures up to the maximum pressure of 500 kPa. The uptake data obtained during the transient period and at equilibrium were subsequently used for the analyses of CO_2 adsorption kinetics and pore texture of the chars, respectively.

Table 1: Proximate and ultimate analyses of coconut shell used in this study.

Proximate analysis (dry basis), wt%	
Volatile matter	80.80
Fixed carbon	19.07
Ash content	0.13
Ultimate analysis, wt%	
C	49.75
H	5.60
O (by diff.)	44.28
N	0.35
S	0.02

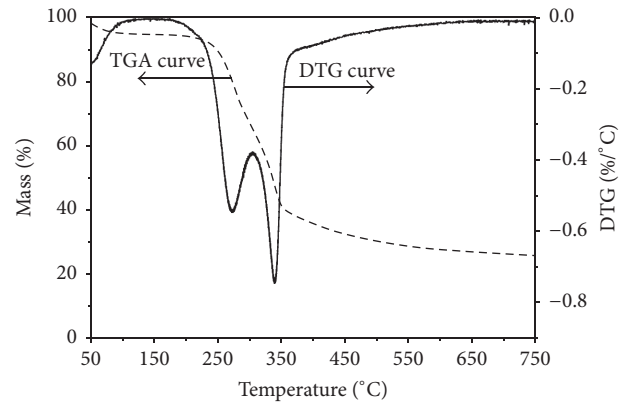

Figure 1: TGA and DTG curves of coconut shell used in this study.

3. Results and Discussion

3.1. Proximate and Ultimate Analyses of Coconut Shell. Table 1 presents the proximate and ultimate analyses of the raw coconut shell used in this work. The results indicate that coconut shell contains a high content of volatile matter with low compositions of ash and sulfur, and carbon and oxygen are the major elements. The fixed carbon content of 19.07% is comparable to those of some biomass materials, for example, longan seed (19.61%) [16], oil palm fiber (18.23%) [17], palm kernel cake (16.74%) [18], palm shell (19.20%) [19], and eucalyptus wood (18.30%) [20].

3.2. TGA and DTG Analysis of Coconut Shell. Nonisothermal thermogravimetric analysis was used to determine the thermal degradation behavior of coconut shell and the results are presented in Figure 1, as weight percent remaining (TG curve)

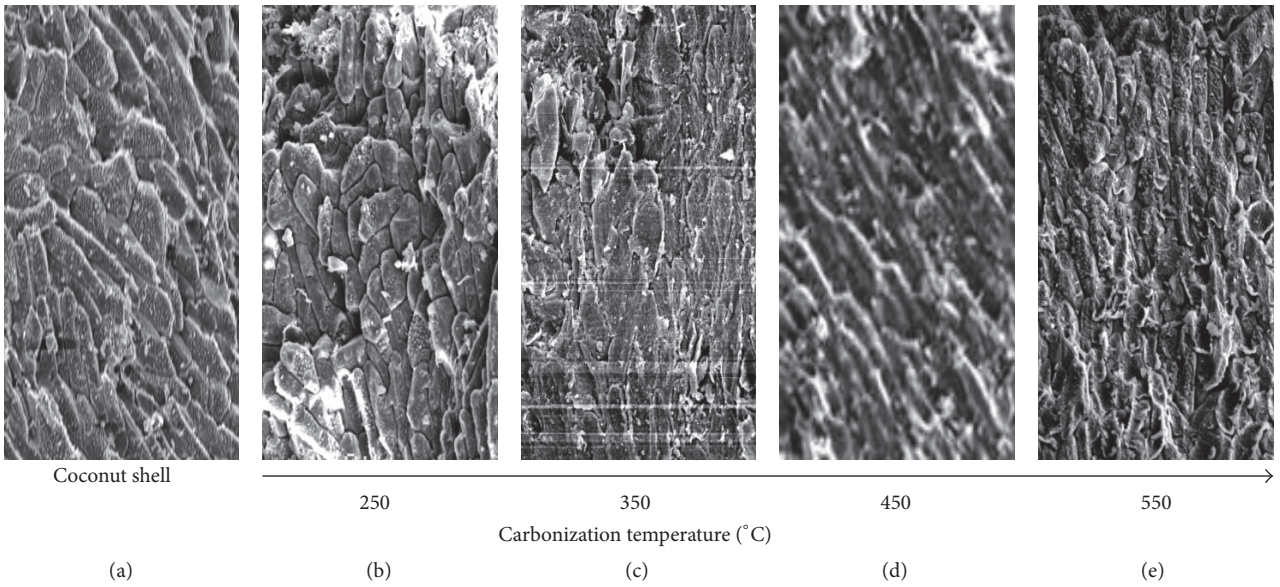

Figure 2: SEM images of coconut shell and coconut shell chars prepared at various carbonization temperatures.

and its corresponding first derivative (DTG curve). The small first peak of the DTG curve which occurs at a temperature below 120°C should result from the liberation of inherent moisture, giving the weight loss of about 2%. It is then followed by two distinct peaks where the main devolatilization occurs, with the first peak appearing in the range from 200 to 315°C and the second peak from 315 to 385°C. The maximum decomposition rates occur at 265°C and 350°C for the first peak and the second peak, respectively. Generally, the thermal decomposition of biomass results from the decomposition of its lignocellulosic components, including hemicellulose, cellulose, and lignin. Lignin usually decomposes first at a low temperature around 160°C and continues over a wide temperature range up to 900°C [21]. Hemicellulose and cellulose decompose over the temperature range from 200 to 380°C and 250 to 400°C, respectively [22]. Thus, it could be inferred that the appearance of the first peak of DTG curve is attributed mainly to the decomposition of hemicellulose component, giving the weight loss of about 28.5%, followed by the decomposition of cellulose showing the second peak with additional weight loss of 26.6%.

Surface morphology, proximate analysis, and true density were determined for the char products derived from coconut shell.

3.3. Surface Morphology of Chars. Figure 2 shows the SEM images of the raw coconut shell and those of the derived chars prepared at different carbonization temperatures of 250, 350, 450, and 550°C. It appears that the coconut shell surface consists of a stack of parallel solid flakes with relatively smooth surfaces. As the carbonization temperature is increased, the char surface shows an increase in the surface roughness. This is probably caused by the increased rupture of the biomass structure due to the release of more volatile species as the heating temperature is increased.

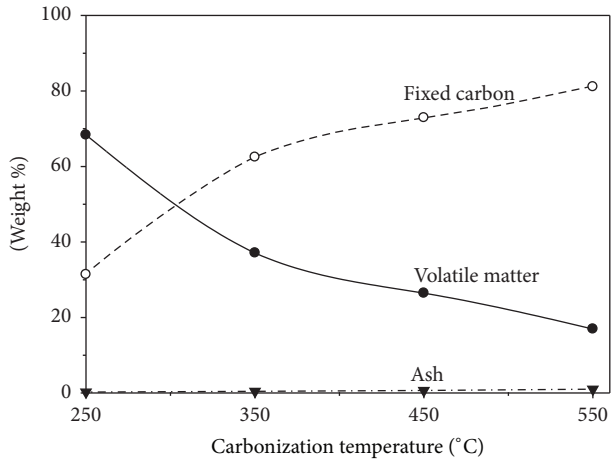

Figure 3: Effect of carbonization temperature on the proximate analysis of coconut shell chars.

3.4. Proximate Analysis of Chars. The effect of the carbonization temperature on chemical compositions of solid chars is displayed in Figure 3. The results show that the volatile content decreases continuously from 68.35% to 15.50% as the carbonization temperature is increased from 250 to 550°C which results from the release of noncarbon elements such as oxygen, nitrogen, hydrogen, and sulfur as volatile gaseous products [23]. As a consequence, the fixed carbon content is increased accordingly from 31.41% to 81.1%. Since the actual mass of ash remains constant over the range of carbonization temperatures studied, the decrease of char yield with an increasing carbonization temperature would cause the ash composition to increase from 0.23% to 1.16%, as shown in Figure 3.

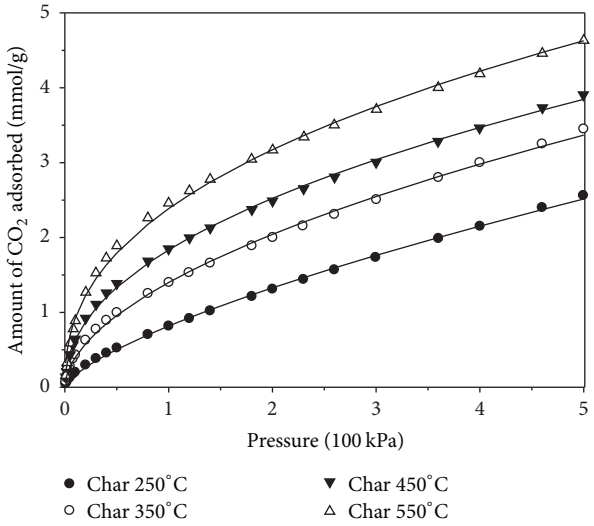

Figure 4: Isotherms of CO_2 adsorption at 273 K by coconut shell chars prepared at various carbonization temperature. The solid lines represent isotherms predicted by the Freundlich and Sips isotherm equations.

3.5. Char Density. Chars prepared at carbonization temperatures of 250, 350, 450, and 550°C possess the true densities of 1.19, 1.28, 1.39, and 1.51 g/cm^3, respectively. Since the yield of char decreases with the increasing carbonization temperature, the increase in the true density of char indicates a certain degree of particle shrinkage. A simple calculation based on char yield and true density data shows that the average spherical diameter of a char particle decreases from 1.16 mm to 0.92 mm (a drop of about 20%) when the carbonization temperature is increased from 250 to 550°C.

3.6. Adsorption Isotherms of CO_2 by Coconut Shell Chars. Figure 4 shows isotherms of CO_2 adsorption at 273 K by coconut shell chars prepared at various carbonization temperatures from 250 to 550°C. Over the applied pressure up to 500 kPa (5 bars), the isotherms exhibit the initial part of Type II isotherm according to the IUPAC classification [24]. With respect to the pressure increasing, two regions of the isotherm curve can be observed, that is, a sharp increase of the amount adsorbed over the initial low pressure range from zero to 10.5 kPa (P/P^o = 0.003, where P^o = saturation vapor pressure of CO_2 at 273 K = 3500 kPa), followed by a continuous increase in the adsorbed amounts with a gradually decreasing slope of the isotherm curve.

The characteristic shape of the Type II isotherm curve suggests that there is a distribution of pore sizes even for chars with a relatively small pore volume. The adsorption of CO_2 at low pressure range possibly involves the adsorption in small narrow micropores of a few molecular dimensions of the adsorptive molecules, known as primary micropore filling [25]. Our simulation study of CO_2 adsorption in porous carbons using a slit-pore model [26] has revealed that the adsorption by the primary pore filling effect occurred for pore width less than 0.85 nm, in comparison with the collision diameter of CO_2 of 0.303 nm. Carbon dioxide adsorption at pressures higher than 10.5 kPa occurs in wider supermicropores (1.4 to 2.0 nm) by quasi-multilayer adsorption due to adsorbate-adsorbate interaction, known as the secondary micropore filling mechanism [25]. It is also interesting to note that the Type II isotherm found for CO_2 adsorption in coconut shell chars was also observed by a number of investigators for CO_2 adsorption in activated carbons having much larger internal surface area [27–30]. This indicates that the basic interaction forces between CO_2 and carbon surfaces in solid chars and activated carbons are fundamentally similar, involving the attraction-repulsion dispersive forces and Coulombic forces induced by the quadrupole moments of CO_2 molecules [31].

An attempt was also made in this work to fit the experimental isotherm data with available adsorption isotherm models. Two popularly used empirical isotherm equations were tested, namely, the two-parameter Freundlich equation and the three-parameter Sips equation [32]. The Freundlich isotherm equation was developed based on the assumption that the surface is heterogeneous; that is, the adsorbent-adsorbate interaction energy is distributed and the surface is grouped into various patches with each patch having its own adsorption energy.

The Freundlich isotherm has the following form:

$$q_F = K_F (P)^{1/n_F}, \quad (1)$$

where q_F is amount of CO_2 adsorbed, mmol/g, P is pressure, kPa, K_F is affinity constant, and n_F is surface heterogeneity constant.

This isotherm equation has no Henry law (linear) behavior at low pressure and no saturation limit at high pressure.

Sips equation takes the form

$$q_S = \frac{q_m (bP)^{1/n_S}}{1 + (bP)^{1/n_S}}, \quad (2)$$

where q_S and q_m are amount adsorbed and monolayer adsorbed capacity in mmol/g, respectively, P is pressure, kPa, b is affinity constant, and n_S is heterogeneity constant.

This isotherm equation combines the characteristics of the Langmuir and Freundlich equations, thus showing a finite adsorption limit when the pressure is sufficiently high.

Table 2 shows the best fitted parameters of the Freundlich and Sips isotherm equations for CO_2 adsorption at 273 K by coconut shell chars prepared at various carbonization temperatures. As seen from Figure 4 and the values of regression coefficient (R^2) in Table 2, the isotherm data are very well described by both adsorption models. It is interesting to observe that the surface heterogeneity constants, n_F and n_S, tend to increase with increasing carbonization temperatures. This result is possibly attributed to the increasing number of surface active sites containing unpaired electrons caused by the increasing degree of bond rupture during the devolatilization of chars [33]. The adsorbed capacity constants, K_F and q_m, also increase with the increase of carbonization temperature, indicating the consequent increase of available surface area for CO_2 adsorption. However, the affinity constant, b, of the Sips equation shows a decrease as the carbonization temperature is increased.

Table 2: Fitted parameters of Freundlich and Sips isotherm equations for CO_2 adsorption at 273 K by coconut-shell chars prepared at various carbonization temperatures.

Carbonization temperature (°C)	Freundlich equation			Sips equation			
	K_F	n_F	R^2	q_m	b	n_s	R^2
250	0.0327	1.43	0.9991	30.4	7.4×10^{-5}	1.37	0.9985
350	0.1130	1.83	0.9988	32.3	4.8×10^{-5}	1.73	0.9981
450	0.2192	2.17	0.9987	47.4	1.3×10^{-5}	2.08	0.9987
550	0.3577	2.43	0.9968	97.7	2.0×10^{-6}	2.36	0.9980

3.7. Pore Characterization of Coconut Shell Chars. Gas adsorption of a single adsorptive molecule is still the most widely used method for the characterization of porous solids. The required information is the surface area and pore size distribution which can be achieved by the application of adsorption theories to the derived isotherm data. For microporous materials like solid chars or activated carbons, the micropore volume and surface area can be assessed, for example, by the well-known equations such as the Dubinin-Radushkevich (DR) equation and the Dubinin-Astakhov (DA) equation or by employing the techniques of t-plot and α_s-plot [10]. The pore size distribution can be determined by the MP method [34] and the Horvath-Kawazoe (HK) method [35] or by more modern techniques of the density functional theory (DFT) [36] or the grand canonical Monte Carlo simulation (GCMC) [37]. In this work only the DR equation and GCMC simulation were used to determine the porous properties of coconut shell chars derived at different carbonization temperatures based on CO_2 adsorption isotherms at 273 K.

The DR equation was developed based on the potential theory of Polanyi [38] to account for the adsorption in microporous solids by the micropore filling mechanism. The cumulated volume of the adsorbed phase is a function of the adsorption potential and this relationship is called the characteristic curve. To obtain the isotherm equation, Dubinin [39] has proposed the specific empirical functional form of the characteristic curve for microporous adsorbents such as activated carbon. The final form of DR equation reads

$$\frac{V}{V_o} = \exp\left[-\frac{\left[RT\ln\left(P^o/P\right)\right]^2}{\beta {E_o}^2}\right] \tag{3}$$

or in linear form,

$$\log V = \log V_o - 2.303\left(\frac{RT}{\beta E_o}\right)^2 \log^2\left(\frac{P^o}{P}\right), \tag{4}$$

where V is the amount adsorbed at pressure P, mmol/g adsorbent, V_o is the amount adsorbed at the saturation pressure P^o, mmol/g, R is gas constant = 8.314×10^{-3} kJ/mol-K, T is adsorption temperature, K, E_o is characteristic energy, kJ/mol, β is scaling factor that brings the characteristic curves for different adsorbates into a single curve, taken as 0.35 for carbon adsorbents.

The plotting of (4) from isotherm data should yield a straight line and the values of E_o and V_o are obtained from the slope and intercept, respectively. The micropore volume (V_{mic}) of the adsorbent (coconut shell chars) is obtained by converting V_o into the volume of adsorbate in liquid state (liquid density of CO_2 is 0.0207 mol/cm^3) and the micropore area (A_{mic}) in m^2/g can be calculated from V_o by the equation

$$A_{\text{mic}} = V_o a_m N_a, \tag{5}$$

where V_o is the micropore adsorbed capacity (mol/g), a_m is the cross-sectional area of CO_2 (2.1×10^{-9} m^2/molecule at 273 K), and N_a is the Avogadro number (6.02×10^{23} molecules/mol).

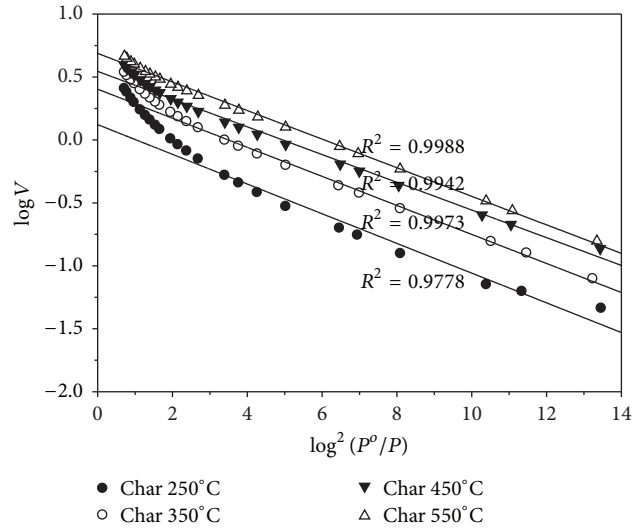

Figure 5: DR plots for CO_2 adsorption at 273 K by coconut shell chars prepared at different carbonization temperatures (P^o = 3500 kPa for CO_2 at 273 K).

The calculation method used for the characterization of porous chars by the GCMC simulation is that proposed by Herrera et al. [40]. The set of simulated isotherms are generated using the technique of grand canonical Monte Carlo simulation for carbon dioxide adsorption at 273 K, based on the slit-pore model (parallel graphitic surfaces) with pore width varying from 0.55 to 3 nm. The experimental isotherms and those of simulated results are then matched by using an optimization function of the MATLAB code to arrive at a pore volume for each pore size as well as its surface area. The pore size distribution, the average pore size (D_{av}), the cumulated surface area, and the total pore volume are then calculated.

Figure 5 shows the DR plots for CO_2 adsorption at 273 K by coconut shell chars prepared at various carbonization temperatures. The linear fitting is satisfactory over a low

Table 3: Calculated porous properties of coconut-shell chars prepared at various carbonization temperatures based on DR equation and GCMC simulation method.

Carbonization temperature (°C)	DR equation			GCMC simulation		
	V_{mic} (cm^3/g)	A_{mic} (m^2/g)	E_o (kJ/mol)	V_{mic} (cm^3/g)	A_{mic} (m^2/g)	D_{av} (nm)
250	0.064	167	28.7	0.079	285	1.25
350	0.122	320	29.0	0.125	356	1.45
450	0.169	443	29.7	0.153	418	1.46
550	0.217	566	29.9	0.189	503	1.47

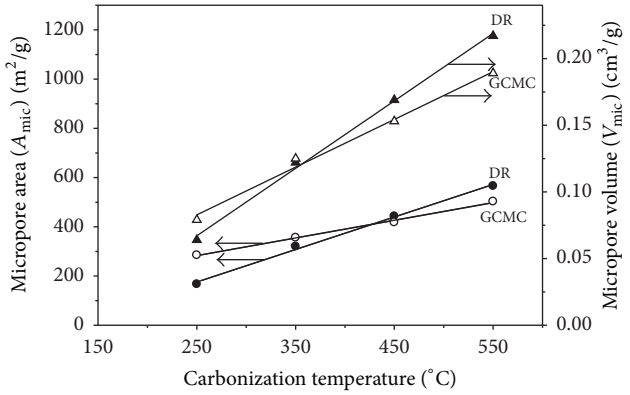

Figure 6: Effect of carbonization temperature on the porous properties of coconut shell chars, calculated by DR equation and GCMC simulation.

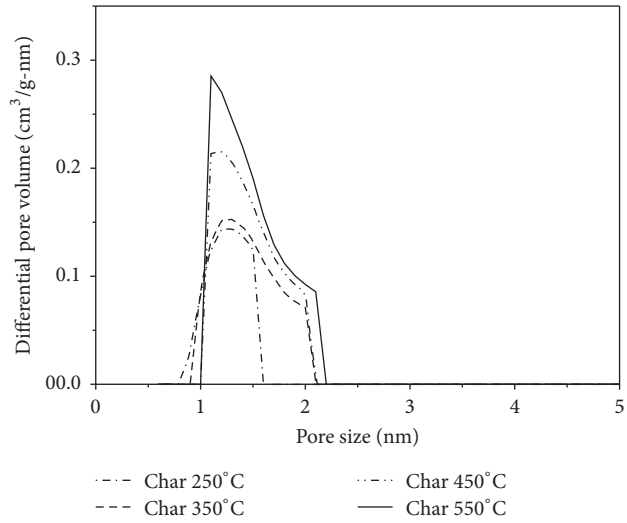

Figure 7: Pore size distribution of coconut shell chars prepared at various carbonization temperatures calculated by GCMC simulation technique.

pressure range where adsorption takes place by micropore filling in small micropores (pore size < 1.4 nm). However, at higher pressures the experimental isotherms tend to deviate from linearity showing an upward turn toward the y-axis and this characteristic corresponds to adsorption in larger supermicropores or some mesopores [41]. The pressure at which the isotherm points start to bend upward appears to increase with increasing carbonization temperatures, having the values of about 100 kPa for the 250°C char and 400 kPa for the 550°C char. The increase of this threshold pressure indicates that the char of a higher carbonization temperature contains a larger volume of small micropores, as compared to that of the lower carbonization temperature char, thus enabling the adsorption to proceed to a higher pressure. Evidence to support this view is seen from Figure 7 for the pore size distribution of chars, as will be discussed later on.

Table 3 and Figure 6 show the porous properties of coconut shell chars estimated by the DR equation and the GCMC simulation. The results on the micropore volume and micropore area of coconut shell chars derived from DR equation and GCMC simulation agree reasonably well, differing on average by about 10% except for the lowest carbonization temperature char that gives 20% and 70% differences for the micropore volume and micropore area, respectively. Porous properties of chars increase linearly with the increase of carbonization temperature from 250 to 550°C. This suggests that over this temperature range the creation of internal pores basically involves the primary decomposition of biomass components of coconut shell, probably without secondary reactions such as thermal cracking, repolymerization, and recondensation of devolatilization products that could occur at higher temperatures [18].

The DR equation gives the largest range of micropore volume and micropore area varying from 0.064 to 0.217 cm^3/g and 167 to 566 m^2/g, respectively, when the carbonization temperature is increased from 250 to 550°C. It is also noted that over this temperature range the average pore diameter of chars as determined by GCMC simulation method increases from 1.25 to 1.47 nm, indicative of pore enlargement by the effect of increasing carbonization temperature.

Results on pore size distribution of coconut shell chars estimated by the GCMC simulation are presented in Figure 7. It is seen that the pore size distributions of all chars are in the range from 0.8 to 2.2 nm. There is a tendency for the distribution to become wider as the carbonization temperature is increased but the difference is not pronounced, being in the ranges 0.8 to 1.6 nm, 0.9 to 2.0 nm, 0.9 to 2.1 nm, and 1.0 to 2.2 nm for chars carbonized at 250, 350, 450, and 550°C, respectively. All pores of the 250°C char are micropores (pore size < 2 nm), while chars of higher carbonization temperatures contain mostly micropores with around 5% being in the mesopore size range (2 to 50 nm). It is noted that the volume of micropores smaller than 1.4 nm, which

is responsible for the major adsorption by micropore filling, tends to increase with increasing carbonization temperature, in support of the previous discussion on the deviation from linearity of the DR plots.

3.8. Adsorption Kinetics of CO_2 and Diffusivity Equations. The kinetic analysis for CO_2 adsorption by coconut shell char is obtained by writing a mass balance equation for the transport of an adsorbate molecule inside a single spherical adsorbent particle [42], as shown in

$$\frac{\partial q}{\partial t} = D_e \left[\frac{\partial^2 q}{\partial r^2} + \frac{2\partial q}{r\partial r} \right], \tag{6}$$

where $q(t)$ is the adsorbate concentration, D_e is the effective pore diffusivity, and r is the radial distance. Upon solving (6) using appropriate initial and boundary conditions, the final solution gives the concentration of adsorbate as a function of time and radial position inside the particle, $q = q(r, t)$.

The solution equation for the fractional uptake of the adsorbate (F) is then given by the equation

$$\begin{aligned} F &= \frac{\overline{q}_{(t)} - q_{(0)}}{q_e - q_{(0)}} \\ &= 1 - \left(\frac{6}{\pi^2}\right) \sum_{n=1}^{\infty} \left(\frac{1}{n^2}\right) \exp\left[\frac{-n^2\pi^2 D_e t}{{R_P}^2}\right], \end{aligned} \tag{7}$$

where $\overline{q}_{(t)}$ is average concentration of adsorbate in the particle at time t given as follows:

$$\overline{q}_{(t)} = \frac{3}{{R_P}^3} \int_0^{R_P} q_{(t)} r^2 dr, \tag{8}$$

where R_P is particle radius = 0.72 mm, $q_{(0)}$ is initial concentration of adsorbate, taken as zero for a fresh adsorbent, and q_e is adsorbate concentration at equilibrium, obtained from an isotherm equation.

To facilitate the calculation, only the first two terms of the series solution in (7) are used. This gives

$$\begin{aligned} F = 1 &- \left(\frac{6}{\pi^2}\right) \\ &\cdot \left[\exp\left(\frac{-\pi^2 D_e t}{{R_P}^2}\right) + \left(\frac{1}{4}\right) \exp\left(\frac{-4\pi^2 D_e t}{{R_P}^2}\right) \right]. \end{aligned} \tag{9}$$

Typical kinetic data obtained during the transient measurement by the IGA are shown plotted in Figure 8. These data were fitted with (9) using a nonlinear regression algorithm to obtain the best fit of the effective pore diffusivity (D_e) in the equation as a function of applied pressure.

The correlation between D_e and the equilibrium adsorption loading of CO_2 (q_e) can now be obtained by converting the pressure to q_e via the Freundlich isotherm equation and the results are delineated in Figure 9. As seen, char prepared at a higher carbonization temperature has a higher value of diffusivity for all adsorption loading, due principally to its larger pore size and pore volume. Further, the pore

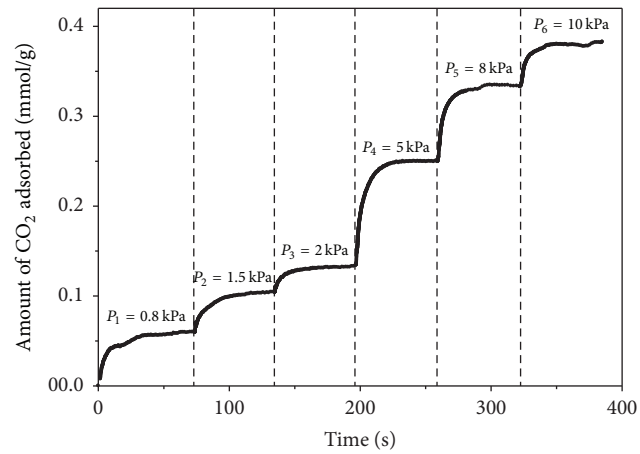

FIGURE 8: Typical uptake of CO_2 adsorption at 273 K by coconut shell char as a function of adsorption time and applied pressure measured by the IGA instrument.

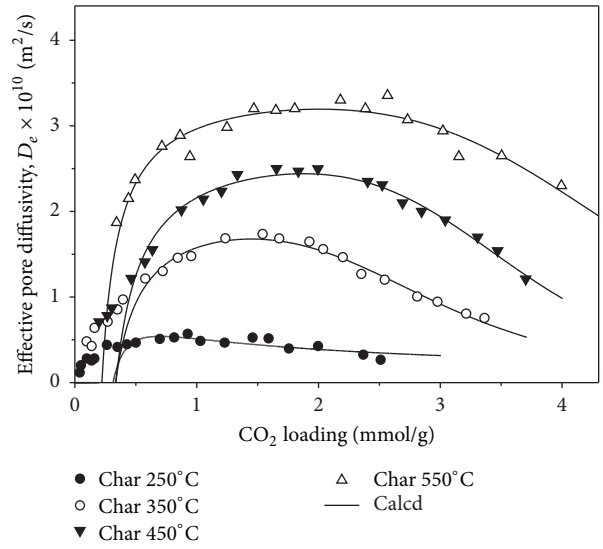

FIGURE 9: Effect of CO_2 loading on effective pore diffusivity (D_e) of CO_2 at 273 K in coconut shell chars prepared at various carbonization temperatures.

diffusivity increases with increasing CO_2 loading and passes through a maximum ($D_{e,\max}$) at an optimum value of q_e (q_{op}). The values of $D_{e,\max}$ and the corresponding q_{op} are 5.40×10^{-11} m^2/s and 0.70 mmol/g, 1.68×10^{-10} m^2/s and 1.54 mmol/g, 2.44×10^{-10} m^2/s and 1.87 mmol/g, and 3.19×10^{-10} m^2/s and 2.10 mmol/g for chars prepared at the carbonization temperatures of 250, 350, 450, and 550°C, respectively. The drop of the pore diffusivity is obviously caused by the blocking of pore space when the adsorption loading is sufficiently high and this pore blocking effect persists to a higher optimum loading as the carbonization temperature is increased. It should be noted that the value of $D_{e,\max}$ (3.19×10^{-10} m^2/s) for CO_2 adsorption in the 550°C char is about two orders of magnitude smaller than the CO_2 diffusivity at 308 K (2.61×10^{-8} m^2/s) in BPL activated carbon [42], indicative of

Table 4: Values of constants in (18) for predicting the effective pore diffusivity of CO_2 (D_e) at 273 K in various coconut shell chars.

Carbonization temperature (°C)	t_e	C_1	C_2	C_3	C_4	R^2
250	0.38	−0.06	80.5	4×10^{-6}	0.60	0.6805
350	228	−0.37	182	2.92	4.21	0.9733
450	168	0.25	−15.5	3.61	5.44	0.9725
550	137	−0.28	132	4.57	4.94	0.8923

lower pore diffusional resistance of activated carbon due to its more developed and well-connected pore structure.

An attempt is now made to estimate the pore size at which the diffusivity starts to decline (D_{op}) for all chars. By assuming a cylindrical pore of length L and an average diameter D_{av}, the pore volume (V_T) is given by

$$V_T = \left(\frac{\pi}{4}\right) {D_{av}}^2 L. \tag{10}$$

The adsorbed volume corresponding to q_{op} (V_{op}) can be calculated from the product of a cross-sectional area of the adsorbed layer and the pore length, so that

$$V_{op} = \left(\frac{\pi}{4}\right) \left({D_{av}}^2 - {D_{op}}^2\right) L. \tag{11}$$

Eliminating L from (10) and (11) and rearranging the terms give

$$D_{op} = D_{av} \left(1 - \frac{V_{op}}{V_T}\right)^{1/2}, \tag{12}$$

where V_{op} is q_{op}/ρ_L and ρ_L is the density of liquid carbon dioxide.

By employing (12), the values of D_{op} are estimated to be 0.86, 0.95, 0.99, and 1.07 nm, for the carbonization temperatures of 250, 350, 450, and 550°C, respectively. If we consider that the variation of D_{op} is not so great, the average value of about 1 nm indicates that the pore resistance comes into effect when the adsorption continues until the pore size reduces to approximately three times the collision diameter (size) of the CO_2 molecule.

Finally, it is worthwhile to have a mathematical function to describe the relationship between the effective pore diffusivity and equilibrium loading of CO_2. This is first accomplished by writing down the following three related expressions:

(1) The adsorption rate equation based on the linear driving force (LDF) model [43],

$$\frac{\partial \overline{q}}{\partial t} = \frac{15 D_e \left(q^* - q\right)}{{R_P}^2}, \tag{13}$$

where q^* is the adsorbed-phase concentration in equilibrium with the adsorbate concentration in the bulk phase.

(2) The adsorption kinetic equation of (7), considering only the first term of the series, that is,

$$\overline{q} = q_e \left[1 - \left(\frac{6}{\pi^2}\right) \exp\left(\frac{-\pi^2 D_e t}{{R_P}^2}\right)\right]. \tag{14}$$

(3) The equation for calculating the average adsorbed phase concentration $\overline{q}$ which is derived by integrating (8), assuming a parabolic concentration profile of the adsorbate in the adsorbent particle ($q = C_1 + C_2 r^2$). Thus,

$$\overline{q} = C_1 + 0.6 C_2 {R_P}^2, \tag{15}$$

where C_1 and C_2 are equation constants.

By combining (13) to (15) and considering the condition at equilibrium, $t = t_e$, and $q^* = q_e$, the diffusivity equation as a function of CO_2 loading is finally obtained,

$$D_e = \left(\frac{5.25 \times 10^{-8}}{t_e}\right) \cdot \ln\left[\frac{q_e - C_1 - 3.11 \times 10^{-3} C_2}{0.4 q_e}\right], \quad \mathrm{m^2/s}. \tag{16}$$

However, this functional equation predicts a continued increase of D_e with q_e. To account for the fall of D_e at a certain CO_2 loading, (16) is modified by multiplying with an empirical equation,

$$Q = \frac{1}{\left[1 + \left(q_e/C_3\right)^{C_4}\right]}, \tag{17}$$

where C_3 and C_4 are constants.

As a result, the final equation for describing the effective pore diffusivity as a function of equilibrium CO_2 loading for the adsorption of CO_2 at 273 K by coconut shell chars is

$$D_e = \frac{\left(\left(5.25 \times 10^{-8}\right)/t_e\right) \ln\left[\left(q_e - C_1 - 3.11 \times 10^{-3} C_2\right)/0.4 q_e\right]}{\left[1 + \left(q_e/C_3\right)^{C_4}\right]}, \tag{18}$$

D_e in m^2/s and q_e in mmol/g.

The four constants in (18), being dependent on the carbonization temperature, are then determined by fitting the equation against the diffusivity data employing a nonlinear regression technique and the results are listed in Table 4. The predictive capability of the proposed equation is shown in Figure 9. Overall, the agreement between the computed and experimental values is satisfactory but the equation fails to predict the experimental results for CO_2 loading less than about 0.32 mmol/g of char from which the adsorption takes place in very small pores.

4. Conclusions

Porous properties of coconut shell chars prepared at carbonization temperatures in the range from 250 to 550°C were determined from the isotherm data of CO_2 adsorption at 273 K and pressures up to 500 kPa, employing the DR equation and GCMC simulation. It was found that all chars contain largely micropores with a small percent being in the mesopore size range. The range of pore size distribution tends to increase with increasing carbonization temperature and varies from 0.8 to 2.2 nm. The micropore volume, micropore area, and average pore size appear to increase with the increase of carbonization temperature, being in the range of 0.064 to 0.217 cm^3/g, 167 to 566 m^2/g, and 1.25 to 1.47 nm, respectively, for carbonization temperatures varying from 250 to 550°C. The adsorption kinetics of CO_2 in the pores of a coconut shell char is well described by the diffusional transport model and the characteristic effective pore diffusivity increases with increasing CO_2 loading, showing a maximum at an optimum adsorption loading. The maximum pore diffusivity shifts to a higher loading as the carbonization temperature is increased, giving the values of 5.4×10^{-11} m^2/s at 0.70 mmol/g loading for 250°C char to 3.19×10^{-10} m^2/s at 2.10 mmol/g loading for 550°C char. A semiempirical correlation was proposed to predict the variation of the pore diffusivity with the equilibrium loading of CO_2 adsorption.

Competing Interests

The authors declare that there is no conflict of interests concerning the publication of this paper.

Acknowledgments

The authors gratefully acknowledge the financial support for this work from the Research and Development Fund, Suranaree University of Technology.

References

[1] T. Kan, V. Strezov, and T. J. Evans, "Lignocellulosic biomass pyrolysis: a review of product properties and effects of pyrolysis parameters," *Renewable and Sustainable Energy Reviews*, vol. 57, pp. 1126–1140, 2016.

[2] A. Sharma, V. Pareek, and D. Zhang, "Biomass pyrolysis—a review of modelling, process parameters and catalytic studies," *Renewable and Sustainable Energy Reviews*, vol. 50, pp. 1081–1096, 2015.

[3] T. Aysu and M. M. Küçük, "Biomass pyrolysis in a fixed-bed reactor: effects of pyrolysis parameters on product yields and characterization of products," *Energy*, vol. 64, pp. 1002–1025, 2014.

[4] F.-X. Collard and J. Blin, "A review on pyrolysis of biomass constituents: mechanisms and composition of the products obtained from the conversion of cellulose, hemicelluloses and lignin," *Renewable and Sustainable Energy Reviews*, vol. 38, pp. 594–608, 2014.

[5] Y. Shen, "Chars as carbonaceous adsorbents/catalysts for tar elimination during biomass pyrolysis or gasification," *Renewable and Sustainable Energy Reviews*, vol. 43, pp. 281–295, 2015.

[6] Y. W. Lee, J. Park, C. K. Ryu et al., "Comparison of biochar properties from biomass residues produced by slow pyrolysis at 500°C," *Bioresource Technology*, vol. 148, pp. 196–201, 2013.

[7] A. Alabadi, S. Razzaque, Y. Yang, S. Chen, and B. Tan, "Highly porous activated carbon materials from carbonized biomass with high CO_2 capturing capacity," *Chemical Engineering Journal*, vol. 281, pp. 606–612, 2015.

[8] N. M. Nor, L. C. Lau, K. T. Lee, and A. R. Mohamed, "Synthesis of activated carbon from lignocellulosic biomass and its applications in air pollution control—a review," *Journal of Environmental Chemical Engineering*, vol. 1, no. 4, pp. 658–666, 2013.

[9] J. W. Patricks, *Porosity in Carbons: Characterization and Applications*, Edward Arnold Publisher, 1995.

[10] S. J. Gregg and K. S. W. Sing, *Adsorption, Surface Area and Porosity*, Academic Press, 2nd edition, 1982.

[11] H. Marsh and F. Rodriguez-Reinoso, *Activated Carbon*, Elsevier, 2006.

[12] D. Lozano-Castelló, D. Cazorla-Amorós, and A. Linares-Solano, "Usefulness of CO_2 adsorption at 273 K for the characterization of porous carbons," *Carbon*, vol. 42, no. 7, pp. 1233–1242, 2004.

[13] D. Özçimen and A. Ersoy-Meriçboyu, "Carbonization kinetics of various biomass sources," *Journal of Chemical Engineering Research Updates*, vol. 1, no. 1, pp. 20–28, 2014.

[14] C. Tangsathitkulchai, S. Junpirom, and J. Katesa, "Comparison of kinetic models for CO_2 gasification of coconut-shell chars: carbonization temperature effects on char reactivity and porous properties of produced activated carbons," *Engineering Journal*, vol. 17, no. 1, pp. 13–28, 2013.

[15] D. López-González, M. Fernandez-Lopez, J. L. Valverde, and L. Sanchez-Silva, "Gasification of lignocellulosic biomass char obtained from pyrolysis: kinetic and evolved gas analyses," *Energy*, vol. 71, pp. 456–467, 2014.

[16] S. Junpirom, C. Tangsathitkulchai, and M. Tangsathitkulchai, "Thermogravimetric analysis of longan seed biomass with a two-parallel reactions model," *Korean Journal of Chemical Engineering*, vol. 27, no. 3, pp. 791–801, 2010.

[17] A. C. Lua and J. Guo, "Preparation and characterization of chars from oil palm waste," *Carbon*, vol. 36, no. 11, pp. 1663–1670, 1998.

[18] P. Weerachanchai, C. Tangsathitkulchai, and M. Tangsathitkulchai, "Characterization of products from slow pyrolysis of palm kernel cake and cassava pulp residue," *Korean Journal of Chemical Engineering*, vol. 28, no. 12, pp. 2262–2274, 2011.

[19] P. Luangkiattikhun, C. Tangsathitkulchai, and M. Tangsathitkulchai, "Non-isothermal thermogravimetric analysis of oil-palm solid wastes," *Bioresource Technology*, vol. 99, no. 5, pp. 986–997, 2008.

[20] Y. Ngernyen, C. Tangsathitkulchai, and M. Tangsathitkulchai, "Porous properties of activated carbon produced from Eucalyptus and Wattle wood by carbon dioxide activation," *Korean Journal of Chemical Engineering*, vol. 23, no. 6, pp. 1046–1054, 2006.

[21] H. Yang, R. Yan, H. Chen, D. H. Lee, and C. Zheng, "Characteristics of hemicellulose, cellulose and lignin pyrolysis," *Fuel*, vol. 86, no. 12-13, pp. 1781–1788, 2007.

[22] D. Vamvuka, E. Kakaras, E. Kastanaki, and P. Grammelis, "Pyrolysis characteristics and kinetics of biomass residuals mixtures with lignite," *Fuel*, vol. 82, no. 15–17, pp. 1949–1960, 2003.

[23] R. C. Bansal and M. Goyal, *Activated Carbon Adsorption*, Taylor & Francis, 2005.

[24] S. Lowell, J. E. Shields, M. A. Thomas, and M. Thomas, *Characterization of Porous Solids and Powders: Surface Area, Pore Size and Density*, Kluwer Academic, Dordrecht, the Netherlands, 2004.

[25] F. Rouquerol, J. Rouquerol, and K. Sing, *Adsorption by Powders and Porous Solids*, Academic Press, 1999.

[26] A. Wongkoblap, W. Intomya, W. Somrup, S. Charoensuk, S. Junpirom, and C. Tangsathitkulchai, "Pore size distribution of carbon with different probe molecules," *Engineering Journal*, vol. 14, no. 3, pp. 45–56, 2010.

[27] S. Deng, H. Wei, T. Chen, B. Wang, J. Huang, and G. Yu, "Superior CO_2 adsorption on pine nut shell-derived activated carbons and the effective micropores at different temperatures," *Chemical Engineering Journal*, vol. 253, pp. 46–54, 2014.

[28] J. Sreńscek-Nazzal, U. Narkiewicz, A. W. Morawski, R. J. Wróbel, and B. Michalkiewicz, "Comparison of optimized isotherm models and error functions for carbon dioxide adsorption on activated carbon,," *Journal of Chemical & Engineering Data*, vol. 60, no. 11, pp. 3148–3158, 2015.

[29] R.-L. Tseng, F.-C. Wu, and R.-S. Juang, "Adsorption of CO_2 at atmospheric pressure on activated carbons prepared from melamine-modified phenol-formaldehyde resins," *Separation and Purification Technology*, vol. 140, pp. 53–60, 2015.

[30] B. B. Saha, S. Jribi, S. Koyama, and I. I. El-Sharkawy, "Carbon dioxide adsorption isotherms on activated carbons," *Journal of Chemical & Engineering Data*, vol. 56, no. 5, pp. 1974–1981, 2011.

[31] Y. Liu and J. Wilcox, "Molecular simulation studies of CO_2 adsorption by carbon model compounds for carbon capture and sequestration applications," *Environmental Science & Technology*, vol. 47, no. 1, pp. 95–101, 2013.

[32] D. D. Do, *Adsorption Analysis: Equilibria and Kinetics*, Imperial College Press, 1998.

[33] W. Li, K. Yang, J. Peng, L. Zhang, S. Guo, and H. Xia, "Effects of carbonization temperatures on characteristics of porosity in coconut shell chars and activated carbons derived from carbonized coconut shell chars," *Industrial Crops and Products*, vol. 28, no. 2, pp. 190–198, 2008.

[34] R. S. Mikhail, S. Brunauer, and E. E. Bodor, "Investigations of a complete pore structure analysis: I. Analysis of micropores," *Journal of Colloid and Interface Science*, vol. 26, no. 1, pp. 45–53, 1968.

[35] G. Horvath and K. Kawazoe, "Method for the calculation of effective pore size distribution in molecular sieve carbon," *Journal of Chemical Engineering of Japan*, vol. 16, no. 6, pp. 470–475, 1983.

[36] P. I. Ravikovitch, G. L. Haller, and A. V. Neimark, "Density functional theory model for calculating pore size distributions: pore structure of nanoporous catalysts," *Advances in Colloid and Interface Science*, vol. 76-77, pp. 203–226, 1998.

[37] S. Samios, A. K. Stubos, N. K. Kanellopoulos, R. F. Cracknell, G. K. Papadopoulos, and D. Nicholson, "Determination of micropore size distribution from grand canonical Monte Carlo simulations and experimental CO_2 isotherm data," *Langmuir*, vol. 13, no. 10, pp. 2795–2802, 1997.

[38] M. Polanyi, "Theories of the adsorption of gases," *Transactions of the Faraday Society*, vol. 28, pp. 316–333, 1932.

[39] M. M. Dubinin, "Adsorption in micropores," *Journal of Colloid and Interface Science*, vol. 23, no. 4, pp. 487–499, 1967.

[40] L. F. Herrera, C. Fan, V. Nguyen, D. D. Do, T. Horikawa, and D. Nicholson, "A self-consistent method to determine accessible volume, area and pore size distribution (APSD) of BPL, Norit and AX-21 activated carbon," *Carbon*, vol. 50, no. 2, pp. 500–509, 2012.

[41] N. Kanellopoulos, *Nanoporous Materials: Advanced Techniques for Characterization, Modeling and Processing*, CRC Press, 2011.

[42] J. A. Delgado, V. I. Águeda, M. A. Uguina, J. L. Sotelo, P. Brea, and C. A. Grande, "Adsorption and diffusion of H_2, CO, CH_4, and CO_2 in BPL activated carbon and 13X zeolite: evaluation of performance in pressure swing adsorption hydrogen purification by simulation," *Industrial & Engineering Chemistry Research*, vol. 53, no. 40, pp. 15414–15426, 2014.

[43] E. Glueckauf, "Theory of chromatography. Part 10.—formula for diffusion into spheres and their application to chromatography," *Transactions of the Faraday Society*, vol. 51, pp. 1540–1551, 1955.